

## All-optical supercontinuum switching

Oliver Melchert<sup>1,2,3</sup>, Carsten Brée<sup>4</sup>, Ayhan Tajalli<sup>1,2</sup>, Alexander Pape<sup>2,5</sup>, Rostislav Arkhipov<sup>6</sup>, Stephanie Willms<sup>1,2</sup>, Ihar Babushkin<sup>1,2</sup>, Dmitry Skryabin<sup>7</sup>, Günter Steinmeyer<sup>8,9</sup>, Uwe Morgner<sup>1,2,3</sup> & Ayhan Demircan<sup>1,2,3</sup>

Efficient all-optical switching is a challenging task as photons are bosons and cannot immediately interact with each other. Consequently, one has to resort to nonlinear optical interactions, with the Kerr gate being the classical example. However, the latter requires strong pulses to switch weaker ones. Numerous approaches have been investigated to overcome the resulting lack of fan-out capability of all-optical switches, most of which relied on types of resonant enhancement of light-matter interaction. Here we experimentally demonstrate a novel approach that utilizes switching between different portions of soliton fission induced supercontinua, exploiting an optical event horizon. This concept enables a high switching efficiency and contrast in a dissipation free setting. Our approach enables fan-out, does not require critical biasing, and is at least partially cascadable. Controlling complex soliton dynamics paves the way towards building all-optical logic gates with advanced functionalities.

<sup>1</sup>Cluster of Excellence PhoenixD, Welfengarten 1, 30167 Hannover, Germany. <sup>2</sup>Institute of Quantum Optics, Leibniz University Hannover, Welfengarten 1, 30167 Hannover, Germany. <sup>3</sup>Hannover Centre for Optical Technologies, Nienburgerstr. 17, 30167 Hannover, Germany. <sup>4</sup>Weierstraß Institute for Applied Analysis and Stochastics, Mohrenstraße 39, 10117 Berlin, Germany. <sup>5</sup>VALO Innovations GmbH, Hollerithallee 17, 30419 Hannover, Germany. <sup>6</sup>St. Petersburg State University, Universitetskaya nab. 7/9, St. Petersburg 199034, Russia. <sup>7</sup>Department of Physics, University of Bath, Bath BA2 7AY, UK. <sup>8</sup>Institut für Physik, Humboldt-Universität zu Berlin, Newtonstraße 15, 12489 Berlin, Germany. <sup>9</sup>Max Born Institute (MBI), Max-Born-Str. 2a, 12489 Berlin, Germany. ✉email: [gunter.steinmeyer@hu-berlin.de](mailto:gunter.steinmeyer@hu-berlin.de); [demircan@iqo.uni-hannover.de](mailto:demircan@iqo.uni-hannover.de)

The bottleneck of most all-optical switching systems is the fan-out capability<sup>1</sup>, that is, one would ideally like to be able to switch several photons with only a single one<sup>2–4</sup>. Even the more modest requirement of switching a photon with exactly one other photon already imposes a major challenge for most photonic switching schemes. One frequently suggested measure against poor switching efficiency is local field enhancement inside a resonant optical cavity<sup>5,6</sup>. However, the resulting increase of the effective nonlinearity comes with a caveat, namely channel separation. Both interacting fields have to be launched collinearly, leaving only the wavelength as a parameter for channel separation<sup>7,8</sup>. Moreover, the resonant nonlinearity enhancement is inevitably accompanied by a decrease in switching speed and an increase of intracavity dispersion, which eventually induces a substantial group delay difference between the two interacting light pulses. Slow light has been suggested as another means for enhancing the interaction time of two pulses in a  $\chi^{(3)}$  nonlinearity<sup>9</sup>, but this idea suffers from some of the same problems as it also requires the introduction of rather large dispersion. A further criterion to allow optical technologies to compete with electronic devices is the switching time. Nowadays efficient all electronic devices with record breaking ultrafast switching times of few picoseconds<sup>10</sup> have been demonstrated. This is on par with demonstrated all-optical concepts, enabling switching times of 1 ps<sup>11</sup>. Recent experiments suggest that all-optical switching times of 260 fs<sup>12</sup> or even below 30 fs<sup>13</sup> may be possible.

Further prospects arise from the rapid development of integrated photonic silicon nitride waveguides, which represent a powerful alternative to nonlinear fibers, and allow on-chip generation of supercontinuum (SC) spectra<sup>14–17</sup>. The underlying physics in these devices is mostly identical, yet their intrinsically higher nonlinearities promise energy scaling by orders of magnitude compared to photonic crystal fibers<sup>18,19</sup>. Specifically, it has recently been shown that microring combs enable data rates of hundreds of terabits per seconds<sup>20</sup>, and it was suggested that cavity solitons from these devices may revolutionize high-speed optical communications<sup>21</sup>. Despite all the progress in the field, one key component is still missing, namely a device that would enable time-division multiplexing at data rates beyond 100 Gbit/s, and this gap could obviously be filled by an all-optical transistor with near-unity fan out.

We recently proposed a concept<sup>22,23</sup> enabling high mutual interaction for all-optical manipulation. Key idea to this concept is an effective enhancement of a  $\chi^{(3)}$  nonlinearity inside a dielectric material without any need for a resonant enhancement. Dispersion properties of almost all dielectric materials enable copropagation of light pulses at two exactly matched wavelengths in opposite dispersion regimes. Dispersive waves (DW) in the normal dispersion temporally stretch upon propagation. In contrast, in the anomalous dispersion regime, short pulses form solitons, which propagate without temporally dispersing over long distances. As solitons maintain a high peak power upon propagation, they increase the refractive index in their immediate surroundings via the weak  $\chi^{(3)}$  Kerr nonlinearity of the dielectric material<sup>24,25</sup>. This effect can lead to deceleration or acceleration of the copropagating DW in the leading or trailing part of the soliton<sup>22,26</sup> and to trapping of the dispersive radiation<sup>19,27</sup>.

The process underlying our switching concept has been strongly inspired by findings in other fields of physics. Fluid dynamics reported a wave reflection process<sup>28</sup>, which has analogously been rediscovered in optics<sup>29</sup>. Earlier, this switching process was discussed as an optical analogy to the event horizon<sup>30</sup>, and has been used to investigate diametric acceleration allowing to mimic interaction with negative masses<sup>31,32</sup>, quantum bouncing in cold atomic clouds<sup>33</sup>, or optical rogue wave emergence<sup>34–36</sup>. The latter example can be understood as quantum

noise induced optical switching, demonstrating the potential for minute fluctuations controlling large optical energies. Moreover, the analogy drawn to the kinetics of an event horizon<sup>30</sup> demonstrates the strength of the interaction process and its potential for applications in optical technologies. However, early experimental realisations have been less efficient than anticipated<sup>37</sup>, and the overall concept is just beginning to develop<sup>38</sup>.

A key point for overcoming the previous shortcomings is the choice of incommensurate frequencies in the nonlinear interaction scheme in order to establish long lasting mutual interaction between two pulses. Consequently, given group-velocity matching of the DW to the soliton, both pulses remain temporally tightly locked, which acts similar to a resonant enhancement of the  $\chi^{(3)}$  interaction, yet avoids the dispersion problems of the microcavity approach. The emerging temporal lock can be exploited for all-optical switching applications<sup>22,39,40</sup>. In particular, it has already been shown that an about seven times smaller DW already suffices to spectrally shift the soliton by its full width at half maximum, i.e., the scheme fulfills the fan-out criterion. However, efficient exploitation of this switching scheme requires pulse parameters which are not immediately accessible with available laser technology.

Here, we experimentally demonstrate that a far more efficient switch can be built when a high order rather than a fundamental soliton is used. When injected near the zero-dispersion wavelength (ZDW) of the fiber, one typically expects to see a rapid decay of the high-order soliton into fundamental ones, i.e., the well-known process of soliton fission<sup>41–45</sup>. Subsequently, the fundamental solitons experience a red shift from the Raman effect<sup>46,47</sup>, which, in combination with four-wave mixing processes, eventually leads to the formation of a SC. Launching a DW into the soliton fission cascade now enables controlled and deterministic modification of the outcome of this highly nonlinear process. In our scheme, soliton and DW play the role of emitter and base of an optical transistor, respectively, and a third wavelength channel acts as the collector. Other than in a conventional bipolar transistor, however, our optical switching scheme does not dissipate energy and is therefore completely conservative.

## Results

### Experimental realization of an optical supercontinuum switch.

For a demonstration of our switching concept, we conducted a series of experiments, in which we launched a soliton and a DW with controllable timing into a fiber. The experimental setup is shown and described in Fig. 1a–d (see “Methods” section for details). Conditions are chosen such that both pulses propagate for a certain propagation distance within the fiber at nearly identical group velocity. Due to the Raman self-frequency shift, therefore the initial conditions slightly deviate from exact group-velocity matching. Moreover, we have chosen wavelengths such that we can additionally benefit from phase matching of the four-wave mixing process, choosing a wavelength of 680 and 810 nm for the DW and the soliton, respectively. Figure 2 visualizes the switching concept with simulations of a simplified interaction process with only one fundamental soliton rather than a SC spectrum. Simulations have been performed for the generalized nonlinear Schrödinger equation (GNLSE) for the complex field envelope<sup>18</sup> as well as for the forward unidirectional propagation equation for the analytic signal<sup>48,49</sup> (see “Methods” section for more detail). Both approaches lead to the same results, showing qualitatively near-perfect agreement with the experiments. Parameters for the fundamental soliton have been taken from the experimentally observed ejected solitons, exhibiting pulse widths in the range of 20 fs. To unveil all different mechanisms involved,

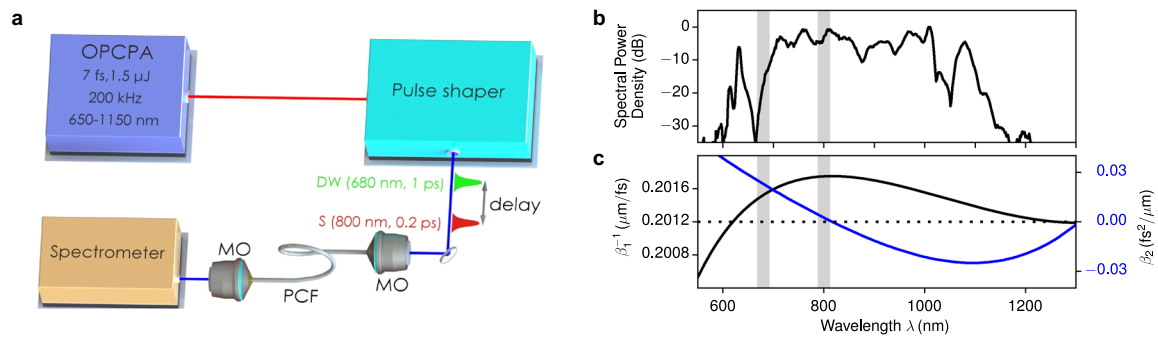


**Fig. 1 Schematic of the experimental setup for all-optical switching.** **a** Optical parametric chirped pulse amplifier (OPCPA) delivers 7 fs pulses with a spectrum spanning from 650 to 1150 nm. Dedicated pulse shaper delivering two pulses, i.e., a dispersive wave (DW) and a higher-order soliton (S), with tunable frequencies and adjustable relative delay. Both pulses are coupled into a photonic crystal fiber (PCF) using a microscope objective (MO). Output of PCF is collimated using a second microscope objective and coupled into a spectrometer. **b** Spectrum of the OPCPA (black line). Gray shaded areas depict wavelengths of soliton and DW that are used as input for interaction process. **c** Inverse group-velocity profile of PCF  $\beta_1^{-1}$  (black line) and resulting group-velocity dispersion  $\beta_2$  (blue line), respectively.

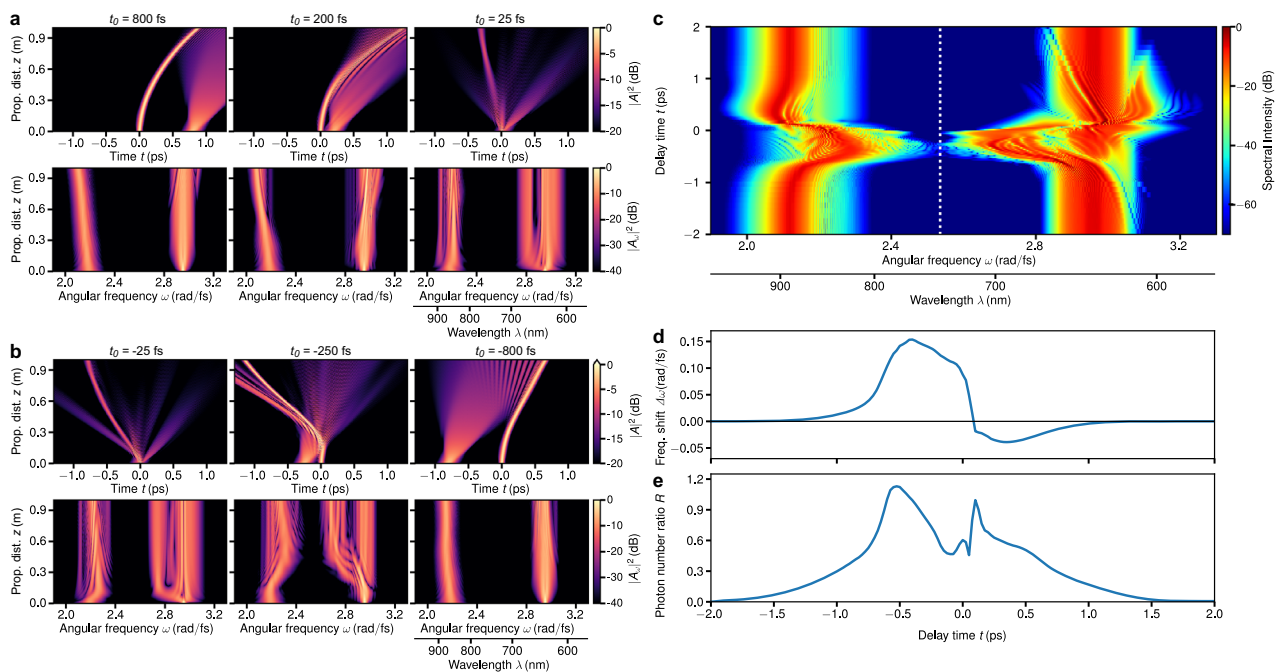


**Fig. 2 Variation of the interaction between one fundamental soliton and a dispersive wave (DW) for different initial time delays.** The initial soliton and DW parameters are kept fixed ( $t_{sol} = 20$  fs,  $\lambda_{sol} = 860$  nm,  $t_{DW} = 70$  fs,  $\lambda_{DW} = 640$  nm) with an intensity ratio of 4/3. **a** Temporal and spectral dynamics for collision processes at the trailing edge of the soliton (initial time delays are superimposed). **b** Corresponding dynamics for collision processes at the leading edge of the soliton (initial time delays are superimposed). A parameter sweep over the initial time delay is shown as Supplementary Movie 1. **c** Output spectra at  $z = 1$  m in dependence of the initial time delay. **d** Induced frequency shift of the soliton in dependence of the delay time demonstrating the efficient manipulation of the soliton in both directions. **e** Extracted energy from the DW involved in the scattering process revealing the different areas of fan-out capability.

we have chosen a relatively high intensity for the DW ( $I_{DW}/I_{sol} = 3/4$ ), which still enables to switch a stronger pulse by a weaker one with respect to the fan-out criterion, identical to the ratio used in the experiments. Figure 2a, the panel denoting  $t_0 = 800$  fs, shows the case where nearly no interaction between the soliton and the DW is initiated. Due to the Raman induced soliton-self-frequency shift, the DW is initially not group-velocity matched to the soliton. With decreasing the delay, see Fig. 2a  $t_0 = 200$  fs panel, group-velocity matched interaction can eventually be realized after propagation for about 0.3 m. In turn, this synchronization leads to a stronger deceleration of the soliton accompanied by a “reflection” of the DW. In the frequency domain, this reflection manifests itself as blue and red shift for the DW and

soliton, respectively. The opposite behavior is observed at initial negative delay at  $t_0 = -50$  fs, as depicted in Fig. 2b. In this exemplary case, one can therefore easily overcome Raman deceleration. The switching dynamics in dependence of time delay are shown in Fig. 2c, with output spectra emerging at  $z = 1$  m. This behavior agrees well with earlier predictions<sup>22,23</sup>.

To explore the fan-out potential of our switching concept, we plotted the frequency shift of the soliton (Fig. 2d), which is representative for the control together with the amount of energy (photon number ratio) of DW/soliton (Fig. 2e). This analysis indicates that significantly lower energies of the DW may be sufficient for controlling the soliton, yet it is also evident that this comes at a price. To this end, we performed a series of

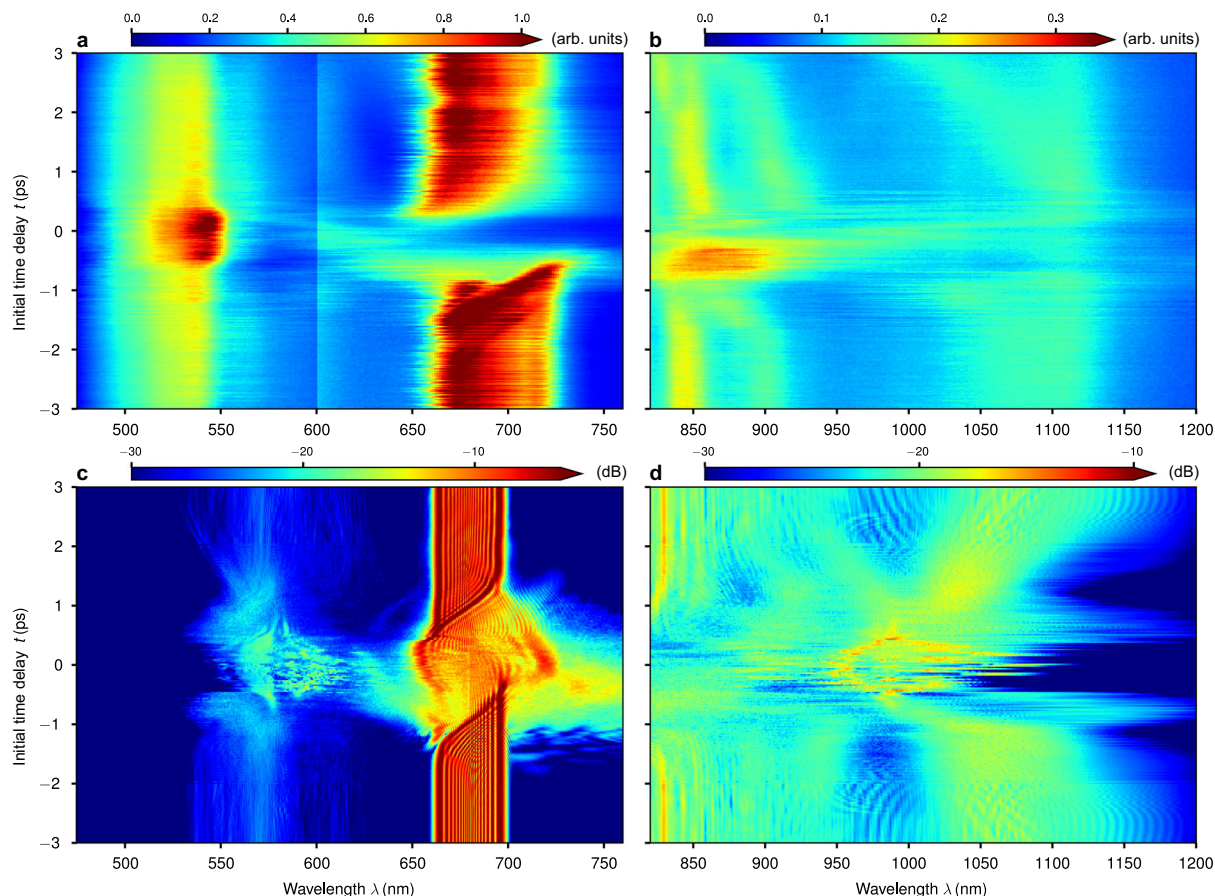


**Fig. 3 Supercontinuum switching with a dispersive wave (DW).** **a** Experimental output spectral range of the DW and **b** of the solitons in dependence on the initial delay between soliton and DW. Two panels were used because measurements were made with two different spectrometers, therefore intensity scales are not immediately comparable. **c, d** Corresponding numerically received output spectra averaged over an ensemble over 100 disorder instances for each time delay. In both cases the switching mechanism appears significantly.

simulations, slowly decreasing the amount of energy of the DW. Soliton control remains down to a ratio 1/5. Further improvement of this record fan-out appears possible with solitons of longer pulse duration. Figure 3a, b depicts the output spectral range, demonstrating resulting frequency shifts for the affected pulses in dependence of their initial time delay in accordance to Fig. 2c. Numerical simulations for comparison are shown in Fig. 3c, d (see below for further details). At large delays, there is no interaction of soliton and DW, and one can observe the undistorted decay of the higher-order soliton. Due to the soliton-self-frequency shift, the first split-off fundamental soliton has experienced a red shift to 1100 nm. A secondary soliton is located at 900 nm.

In our experiments, we used a fiber with two ZDWs. Under these conditions, the second ZDW (ZDW2) of the used fiber at 1250 nm imposes a barrier for further red shifting of the solitons. This effect makes our scenario relatively insensitive to energy fluctuations of the soliton, as the first split-off fundamental soliton will automatically accumulate in a wavelength region below ZDW2. In the language of Miller's criteria<sup>1</sup>, therefore, the choice of a fiber with two dispersion zeros removes the necessity of critical biasing for the 1100 nm output channel. A further advantage results from the fact that the interaction of a DW with a SC has a strong impact on the suppression of rogue solitons<sup>50</sup>.

The center wavelengths of the output solitons can now be manipulated by reducing the initial delay. In particular, launching the DW about 0–500 fs ahead of the soliton (S), the soliton fission process is inhibited, and the spectral content at 1100 nm appears

**Table 1 Optical multigate functionality.**

	Inputs		Outputs (O <sub>i</sub> )		
Designation	DW	S	O <sub>1</sub>	O <sub>2</sub>	O <sub>3</sub>
λ(nm)	680	800	540	680	1100
	0	0	0	0	0
	0	1	0	0	1
	1	0	0	1	0
	1	1	1	0	0
Functionality			S & DW	$\bar{S}$ & DW	S & $\overline{DW}$
Cascadability			-	✓	(✓)

S soliton, DW dispersive wave.

significantly reduced (Fig. 3b). At the same time, the launched DW is completely blue shifted from 680 to 540 nm, and superimposes the much weaker dispersive radiation generated in the fission process (see Fig. 3a). From a switching logic point of view, the output at 540 nm can be considered as S & DW while the 1100 nm output appears when S &  $\overline{DW}$ . The most interesting observation is that input light at 680 nm does not experience any frequency shift when  $\bar{S}$  & DW holds, i.e., this channel is cascadable in the sense of Miller's criteria<sup>1</sup>. At the same time, the 680 nm channel also shows the most impressive switching contrast among all three logical AND functionalities observed. The experimentally observed logic operations are summarized in Table 1 and translated into an equivalent complementary metal

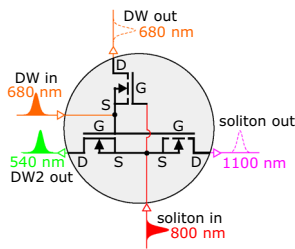


**Fig. 4 Schematic representation of the switching characteristics of the optical transistor, using the symbols of complementary metal oxide semiconductor (CMOS) technology for source (S), drain (D), and gate (G).** These electronic devices come in two variants, which are known as enhancement or depletion type, indicated by either a dashed or solid line between S and drain D, respectively. The situation shown presumes temporal overlap between soliton and input dispersive wave (DW in). In this situation, soliton and DW give rise to a pulse at output port (DW 2), with no output at ports (DW out and soliton out). For other situations, please refer to Table 1.

oxide semiconductor (CMOS) circuitry, consisting of three field-effect transistors, shown in Fig. 4. Our optical transistor enables three parallel operations, does not rely on resonant conditions, and operations can be executed for different combinations of DW and soliton frequencies.

The findings in Fig. 3 are in excellent agreement with the previously suggested concept for an optical transistor<sup>22</sup> and the example shown in Fig. 2, with the noted exception that a much higher soliton order was employed now. Even though the pulse energy ratio of the DW to the soliton is with 3/4 higher than in ref.<sup>22</sup> in our current experimental demonstration, the resulting switching efficiency exceeds the previous predictions, in particular as input channels and output channels of the gate functionalities are now separated by at least 100 nm. In view of the fan-out criterion, we have also to keep in mind, that the DW is used to switch several solitons in parallel and not only one.

**Numerical simulation of the all-optical switch.** To corroborate our experimental findings and understand the dynamics in more detail, we additionally conducted a number of numerical simulations. The output spectra were computed with identical conditions matched to the experiment as best as possible. In particular, as the soliton fission scenario is infamous for its high susceptibility to energy fluctuations on the quantum noise level, we simulated the propagation of pulse ensembles with suitably chosen pulse energy spread. In particular, all major features of the gate functionalities are perfectly reproduced, yet there appear changes in the exact frequency shifts, which we explain by our imperfect knowledge of the exact dispersion properties of the fiber under test. In order to verify this assumption, we performed additional simulations with dispersion profiles differing slightly from the manufacturer specifications. Moreover, we also detect a possible influence of a chirp<sup>51</sup> on the input pulses. Our numerical simulations further indicate that we can adapt the number of output gates by changing input peak intensities.

Figure 5 depicts the temporal and spectral evolution of the interaction for the three exemplary cases, i.e., positive (Fig. 5a), zero (Fig. 5b), and negative (Fig. 5c) initial time delay and the corresponding spectra (Fig. 5d–f), respectively (see also Supplementary Movie 1). Figure 5g–i shows the corresponding cross-correlation frequency-resolved optical gating (XFROG) traces at the output (see “Methods” section for more detail).

In these simulations, one can see that several fundamental solitons are ejected in the process of soliton fission<sup>44</sup>, which are subsequently subject to the interaction with the DW. Depending

on time delay, the solitons are controlled by the DW. It even appears possible to simultaneously control multiple solitons by a single DW, which allows for some adaption of the number of channels in the switching scheme. Specifically, the ejected solitons are accelerated or decelerated due to collisions with a DW at the leading or trailing edges, respectively<sup>22</sup>. This process is accompanied by corresponding shifts in the soliton frequency. Moreover, our simulations indicate the important role of a further four-wave mixing process in the scheme, as mentioned above. Figure 5b, e shows the temporal and spectral dynamics for direct overlapping initial pulses. In the temporal domain it is visible that the soliton fission process itself is affected, namely the ejection of fundamental solitons is inhibited. In the frequency domain, the inhibition enables four-wave mixing mediated generation of two new frequency components  $\omega_1 = 2\omega_{\text{DW}} - \omega_S$  and  $\omega_2 = 2\omega_S - \omega_{\text{DW}}$ . This mechanism can be understood directly from the interaction of one fundamental soliton with a DW at the initial unperturbed frequencies as given in the experiment. In the more complex SC generation process this interaction scenario has even a stronger effect as one can switch on and off the whole process, as demonstrated by the XFROG trace in Fig. 5h (and Supplementary Movie 3). Given that this overall observed behavior may suggest a probabilistic character of the interaction rather than a deterministic action expected of a logic gate, we carefully investigated a large number of simulations, which indicated that collision suppression never fails, see numerically averaged simulations in Fig. 5c, d. As we already described theoretically in ref.<sup>50</sup>, this effect arises due to suppression of solitonic collisions in the presence of an additional DW. We further emphasize that this problem mostly affects the AND functionality of the soliton channel.

## Discussion

We experimentally demonstrated a new route toward optical switching that circumvents most of the complications present in resonant enhancement. Our concept exploits the “event horizon” condition, exploiting higher-order solitons for the implementation of three different all-optical AND gate functionalities with switching times in the femtosecond regime. The logical gate complies with the fan-out criterion<sup>1</sup>, which is difficult to implement otherwise, i.e., we can switch a larger soliton energy by virtue of a DW with less energy. Moreover, critical biasing can be suitably avoided by choosing a fiber with two ZDWs, and the system is immediately cascadable in one of the three output channels. We further expect that a suitable choice of ZDW2 may also enable cascadability for the soliton output channel. Increasing ZDW2 to 1600 nm, one could use an erbium fiber amplifier to restore the soliton energy prior to frequency-doubling it back to 800 nm input wavelength, which may then also enable cascadability of the second input channel. Suitable dispersion engineering provided, it appears conceivable to also exploit other active fibers for mapping the soliton output port back to the DW input. Of course, this will require specifically designed fibers or waveguides. In particular, silicon-based platforms are highly promising, as they promise to lower pulse energies by at least two orders of magnitude compared to our experimental demonstration in this paper. The latter feat enables, e.g., implementation of THz time-division multiplexing schemes with sustainable energy consumption in the few-watt range and may be further improved to sub-watt power levels. In conclusion, while optical logic circuits are certainly still lagging ages behind electronic ones, we nevertheless believe that our experimental demonstration complies with Miller’s rules as best as demonstrated to date. Admittedly, at the same time, we may have barely reached the level that Bardeen and Brattain already demonstrated in the late 1940s:

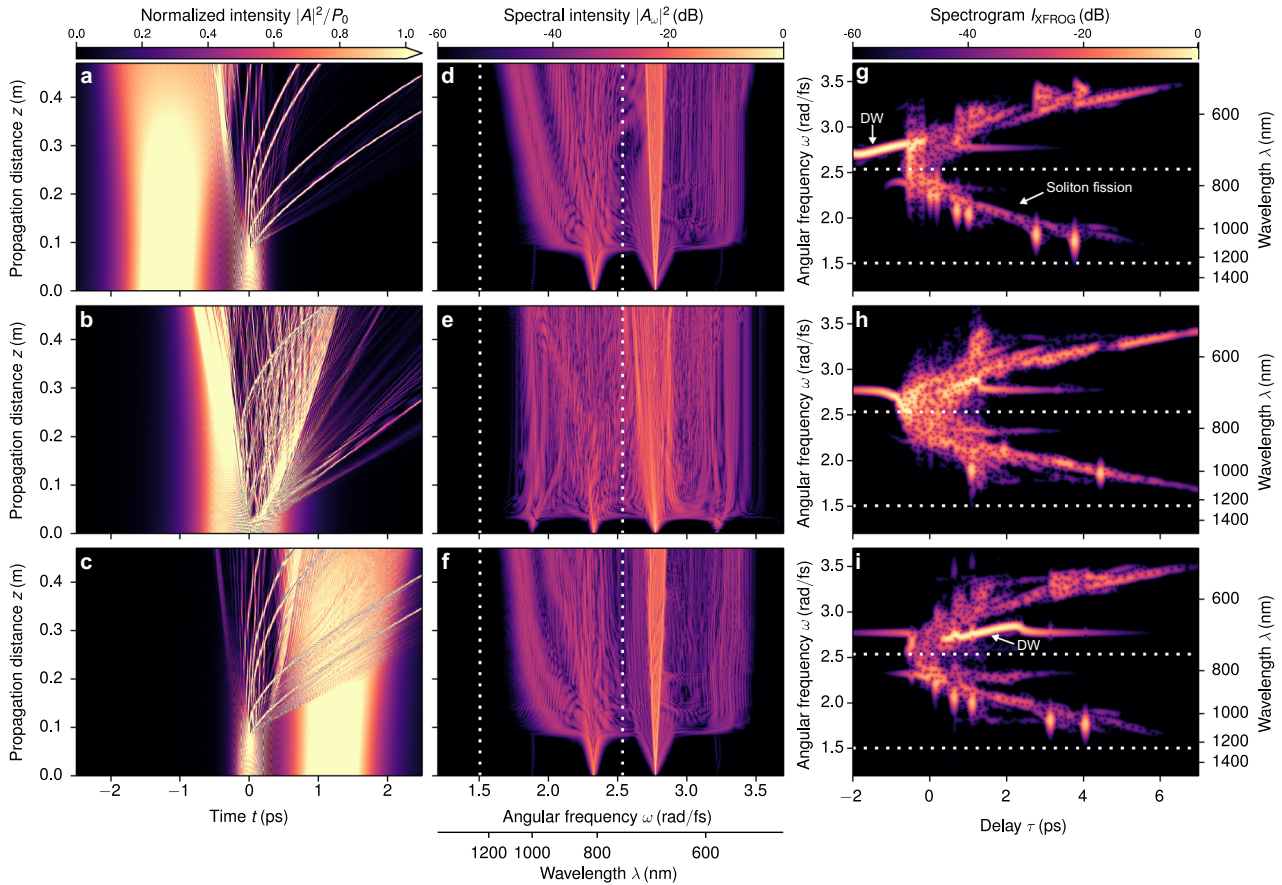


**Fig. 5 Propagation dynamics of the interaction.** **a–c** Temporal and **d–f** spectral evolution (see also Supplementary Movie 2) of the collision process with initial negative, zero, and positive delay, respectively. **g–i** Corresponding cross-correlation frequency-resolved optical gating (XFROG) traces at the output of the fiber (see also Supplementary Movie 3). Negative and positive initial delays lead to acceleration or deceleration of the ejected solitons, whereas the direct superposition involves strong four-wave mixing process, generating new frequencies in combination with the ability to suppress the soliton fission process itself. Clear differences of the scenarios can also be seen in the XFROG traces.

there is still a long way to go from the first experimental demonstration of a Miller-compliant logic gate functionality to a fully functional and useful optical logic circuit.

## Methods

**Experiments.** In our experiments, we used a setup consisting of a noncollinear optical parametric chirped pulse amplification (OPCPA) system delivering energetic broadband pulses and a pulse shaper. The OPCPA delivers sub-7 fs pulses with  $>1.5 \mu\text{J}$  energy operating at 200 kHz repetition rate, with a spectrum spanning from 650 to 1150 nm (see spectrum in Fig. 1). The shaper comprises a pair of knife-edges and two folding mirrors in the Fourier plane of a folded double-pass 4f zero-dispersion line. This setup enables independent selection of two frequency components. The relative delay between the two pulses can be varied by placing one of the folding mirrors on a translation stage with a nominal resolution of 0.2 fs. In addition, one can adjust the energy ratio of the pulses by introducing an attenuator. The gray shaded areas in Fig. 1b, c show the exemplary selected output spectral regions for the experiments using the pulse shaper. The two collinear nJ pulses are then launched by a microscope objective (numerical aperture 0.40) into a 0.47 m long photonic crystal fiber (NKT Photonics, NL-PM-750) with two ZDWs at  $\sim 750$  and 1250 nm, which we refer to as ZDW1 and ZDW2, respectively. Finally, the output of the fiber is analyzed by an optical spectrum analyzer (Ando AQ-6315A).

In the experiments, we launched a DW and a soliton at 680 and 800 nm, respectively. Equal separation from ZDW1 ensures nearly identical group velocities ( $\approx 2.02 \times 10^8$  m/s), with a slightly slower propagation of the DW. The input energy of the 800 nm pulse was adjusted to 1 nJ, which yields a soliton order of  $N = 25$ . Pulse energy of the DW is slightly lower (750 pJ). Pulse duration of the soliton and the DW are 200 fs and 1 ps, respectively.

**Numerical simulations.** Pulse propagation in the photonic crystal fiber is modeled in terms of the slowly varying envelope approximation. Therein,  $z$ -propagation of an initial complex envelope  $A(z = 0, t)$  is accomplished by numerical integration of

the GNLSE:

$$\partial_z A(z, t) = i(\hat{\beta} - \beta_0 - \beta_1 \partial_t) A(z, t) + iy \left( 1 + \frac{i}{\omega_0} \partial_t \right) A(z, t) \int_{-\infty}^{\infty} h(\zeta) |A(z, t - \zeta)|^2 d\zeta,$$

including the effects of dispersion, self-phase modulation, self-steepening and the Raman effect. The above GNLSE resolves the pulse dynamics in a retarded frame of reference moving with group velocity  $v_0 = \beta_1^{-1}$ . Linear dispersion obeys  $(\hat{\beta} - \beta_0 - \beta_1 \partial_t) e^{-i\omega t} = \tilde{\beta}(\omega) e^{-i\omega t}$ , in the Fourier-domain specified by the polynomial approximation  $\tilde{\beta}(\omega) \equiv \sum_{m=2}^{11} \frac{\beta_m}{m!} (\omega + \omega_s - \omega_e)^m$  with expansion coefficients  $\beta_2 = -0.38 \text{ ps}^2 \text{ km}^{-1}$ ,  $\beta_3 = 4.97 \times 10^{-3} \text{ ps}^3 \text{ km}^{-1}$ ,  $\beta_4 = 2.68 \times 10^{-4} \text{ ps}^4 \text{ km}^{-1}$ ,  $\beta_5 = -1.25 \times 10^{-6} \text{ ps}^5 \text{ km}^{-1}$ ,  $\beta_6 = 7.7 \times 10^{-9} \text{ ps}^6 \text{ km}^{-1}$ ,  $\beta_7 = -5.83 \times 10^{-11} \text{ ps}^7 \text{ km}^{-1}$ ,  $\beta_8 = 3.0 \times 10^{-13} \text{ ps}^8 \text{ km}^{-1}$ ,  $\beta_9 = -3.74 \times 10^{-16} \text{ ps}^9 \text{ km}^{-1}$ ,  $\beta_{10} = -7.45 \times 10^{-18} \text{ ps}^{10} \text{ km}^{-1}$ , and  $\beta_{11} = 6.96 \times 10^{-20} \text{ ps}^{11} \text{ km}^{-1}$ , determined for  $\omega_e = 1.85 \text{ rad fs}^{-1}$ . Here,  $\omega$  specifies a frequency detuning with respect to the reference angular frequency  $\omega_s = 2.325 \text{ rad fs}^{-1}$  ( $\lambda_s = 2\pi c_0/\omega_s = 810 \text{ nm}$ ). The assumed nonlinear coefficient is  $\gamma = 3.8 \text{ W}^{-1} \text{ km}^{-1}$ . The group-velocity-dispersion profile  $\beta_2(\omega) = \partial_\omega^2 \tilde{\beta}(\omega)$  exhibits two roots  $\omega_{ZDW1} = 1.505 \text{ rad fs}^{-1}$  ( $\lambda_{ZDW1} = 1252 \text{ nm}$ ) and  $\omega_{ZDW2} = 2.535 \text{ rad fs}^{-1}$  ( $\lambda_{ZDW2} = 743 \text{ nm}$ ) with anomalous dispersion for  $\omega_{ZDW1} < \omega < \omega_{ZDW2}$ .

The total response function in the nonlinear part of the GNLSE includes the instantaneous Kerr and delayed Raman response in the form  $h(t) = (1 - f_R) \delta(t) + f_R h_R(t)$ , with  $f_R = 0.18$  and a Raman-response function:

$$h_R(t) = \frac{\tau_1^2 + \tau_2^2}{\tau_1 \tau_2} e^{-t/\tau_2} \sin(t/\tau_1) \theta(t), \quad (1)$$

with unit step function  $\theta(t)$  and parameter values  $\tau_1 = 12.2 \text{ fs}$ ,  $\tau_2 = 32 \text{ fs}$ . We verified that our findings are reproduced by considering other commonly used Raman-response functions.

For our numerical simulations we consider initial conditions of the form:

$$A(z = 0, t) = A_s \text{sech}\left(\frac{t}{t_s}\right) + A_{\text{DW}} \text{sech}\left(\frac{t + t_0}{t_{\text{DW}}}\right) e^{-i(\omega_s - \omega_{\text{DW}})t}.$$

Therein,  $A_s$ ,  $\omega_s$ , and  $t_s$  are the amplitude, center frequency and duration of the initial soliton pulse. The initial amplitude is defined by the relation

$\gamma A_S^2 = N_S^2 |\beta_2(\omega = 0)| / t_S^2$ , entering the soliton order  $N_S$ . Above,  $A_{DW}$ ,  $\omega_{DW}$ , and  $t_{DW}$  specify the amplitude, center frequency and duration of the DW, injected with a temporal offset  $t_0$  relative to the soliton pulse. The numerical simulations reported in Fig. 2c, d are obtained using the GNLSE with additional quantum noise perturbing the initial condition, i.e.,  $A(z=0, t) \rightarrow A(z=0, t) + \Delta A(t)$ . The complex-valued random noise amplitudes  $\Delta A(t)$  are obtained by spectral synthesis and satisfy the time-domain autocorrelation function  $\langle \Delta A^*(t) \Delta A(t + \tau) \rangle = \hbar \omega_S \delta(t)/2$ , where  $\hbar$  denotes the reduced Planck constant. We verified that the general features of the switching behavior reported in Fig. 1c, d are supported for a wide range of soliton orders  $N_S = 10$ –30 and amplitude ratios  $A_{DW}/A_S < 1$ . The particular numerical results reported in Figs. 1 and 2 are obtained for  $N_S = 17$  and  $A_{DW}/A_S \leq 1$ . The time delay in Fig. 2c, d is shown at increments of 25 fs. For the numerical solution of the GNLSE we use a standard split-step pseudospectral scheme.

The XFROG spectrograms in Fig. 3 are calculated as:

$$I_{\text{XFROG}}(z, \tau, \omega) = \frac{1}{2\pi} \left| \int_{-\infty}^{\infty} A(z, t) h(t - \tau) e^{-i\omega t} dt \right|^2, \quad (2)$$

where the field is localized in time using a Gaussian window function  $h(x) = \exp(-x^2/2\sigma^2)$ , centered at delay time  $t = \tau$  and having root-mean-square width  $\sigma = 50$  fs.

### Data availability

Data supporting the findings reported in this study is available in the Zenodo repository under the link <https://doi.org/10.5281/zenodo.3601387>.

### Code availability

Code that supports the findings reported in this study is available in the Zenodo repository under the link <https://doi.org/10.5281/zenodo.3601362>.

Received: 21 February 2020; Accepted: 24 July 2020;

Published online: 21 August 2020

### References

- Miller, D. A. B. Are optical transistors the logical next step? *Nat. Photon* **4**, 3–4 (2010).
- Chang, D. E., Sørensen, A. S., Demler, E. A. & Lukin, M. D. A single-photon transistor using nanoscale surface plasmons. *Nat. Phys.* **4**, 807–812 (2007).
- Tiarks, D., Baur, S., Schneider, K., Dürr, S. & Rempe, G. Single-photon transistor using a Förster resonance. *Phys. Rev. Lett.* **113**, 053602 (2014).
- Chen, W. et al. All-optical switch and transistor gated by one stored photon. *Science* **341**, 768–770 (2013).
- Hwang, J. et al. A single-molecule optical transistor. *Nature* **460**, 76–80 (2009).
- Gibbs, H. M. *Controlling Light with Light* (Academic Press, 1985).
- Shapiro, J. H. Single-photon Kerr nonlinearly do not help quantum computation. *Phys. Rev. A* **73**, 062305 (2006).
- Volz, J., Scheucher, M., Junge, C. & Rauschenbeutel, A. Nonlinear  $\pi$  phase shift for single fibre-guided photons interacting with a single resonator-enhanced atom. *Nat. Photon.* **8**, 965–970 (2014).
- Shiau, B.-W., Wu, M.-C., Lin, C.-C. & Chen, Y.-C. Low-light-level cross-phase modulation with double slow light pulses. *Phys. Rev. Lett.* **106**, 193006 (2011).
- Nikoo, M. S. et al. Nanoplasma-enabled picosecond switches for ultrafast electronics. *Nature* **579**, 534–539 (2020).
- Huang, C. et al. Ultrafast control of vortex microlasers. *Science* **367**, 1018–1021 (2020).
- Ono, M. et al. Ultrafast and energy-efficient all-optical switching with graphene-loaded deep-subwavelength plasmonic waveguides. *Nat. Photon.* **14**, 37–43 (2020).
- Grinblat, G. et al. Ultrafast sub-30-fs all-optical switching based on gallium phosphide. *Sci. Adv.* **5**, eaaw3262 (2019).
- Halir, R. et al. Ultrabroadband supercontinuum generation in a CMOS-compatible platform. *Opt. Lett.* **37**, 1685 (2012).
- Carlson, D. R. et al. Photonic-chip supercontinuum with tailored spectra for counting optical frequencies. *Phys. Rev. Appl.* **8**, 014027 (2017).
- Wetzel, B. et al. Customizing supercontinuum generation via on-chip adaptive temporal pulse-splitting. *Nat. Commun.* **9**, 4884 (2018).
- Gaeta, A. L., Lipson, M. & Kippenberg, T. J. Photonic-chip-based frequency combs. *Nat. Photon.* **13**, 158–169 (2019).
- Dudley, J. M., Genty, G. & Coen, S. Supercontinuum generation in photonic crystal fiber. *Rev. Mod. Phys.* **78**, 1135 (2006).
- Skryabin, D. V. & Gorbach, A. V. Colloquium: looking at a soliton through the prism of optical supercontinuum. *Rev. Mod. Phys.* **82**, 1287 (2010).
- Hu, H. et al. Single-source chip-based frequency comb enabling extreme parallel data transmission. *Nat. Photon.* **12**, 469–473 (2018).
- Marin-Palomo, P. et al. Microresonator-based solitons for massively parallel coherent optical communications. *Nature* **546**, 274–279 (2017).
- Demircan, A., Amiranashvili, S. & Steinmeyer, G. Controlling light by light with an optical event horizon. *Phys. Rev. Lett.* **106**, 163901 (2011).
- Demircan, A., Amiranashvili, S., Brée, C. & Steinmeyer, G. Compressible octave spanning supercontinuum generation by two-pulse collisions. *Phys. Rev. Lett.* **110**, 233901 (2013).
- Skryabin, D. V. & Yulin, A. V. Theory of generation of new frequencies by mixing of solitons and dispersive waves in optical fibers. *Phys. Rev. E* **72**, 016619 (2005).
- Efimov, A. et al. Interaction of an optical soliton with a dispersive wave. *Phys. Rev. Lett.* **95**, 213902 (2005).
- Driben, R., Mitschke, F. & Zhavoronkov, N. Cascaded interactions between Raman induced solitons and dispersive waves in photonic crystal fibers at the advanced stage of supercontinuum generation. *Opt. Express* **18**, 25993–25998 (2010).
- Gorbach, A. V. & Skryabin, D. V. Light trapping in gravity-like potentials and expansion of supercontinuum spectra in photonic-crystal fibres. *Nat. Photon.* **1**, 653–657 (2007).
- Smith, R. The reflection of short gravity waves on a non-uniform current. *Math. Proc. Camb. Philos. Soc.* **78**, 517 (1975).
- Plansinis, B. W., Donaldson, W. R. & Agrawal, G. P. What is the temporal analog of reflection and refraction of optical beams? *Phys. Rev. Lett.* **115**, 183901 (2015).
- Philbin, T. G. et al. Fiber-optical analog of the event horizon. *Science* **319**, 1367–1370 (2008).
- Batz, S. & Peschel, U. Diametrically driven self-accelerating pulses in a photonic crystal fiber. *Phys. Rev. Lett.* **110**, 193901 (2013).
- Wimmer, M. et al. Optical diametric drive acceleration through action-reaction symmetry breaking. *Nat. Phys.* **9**, 780–784 (2013).
- Gorbach, A. V. & Skryabin, D. V. Bouncing of a dispersive pulse on an accelerating soliton and stepwise frequency conversion in optical fibers. *Opt. Exp.* **15**, 14560 (2007).
- Demircan, A. et al. Rogue events in the group velocity horizon. *Sci. Rep.* **2**, 850 (2012).
- Driben, R. & Babushkin, I. Accelerated rogue waves generated by soliton fission at the advanced stage of supercontinuum formation in photonic-crystal fibers. *Opt. Lett.* **37**, 5157 (2012).
- Saleh, M. F., Conti, C. & Biancalana, F. Anderson localisation and optical-event horizons in rogue-soliton generation. *Opt. Exp.* **25**, 5457 (2017).
- Webb, K. E. et al. Nonlinear optics of fibre event horizons. *Nat. Commun.* **5**, 4969 (2014).
- Drori, J., Rosenberg, Y., Bermudez, D., Silberberg, Y. & Leonhardt, U. Observation of stimulated Hawking radiation in an optical analogue. *Phys. Rev. Lett.* **122**, 010404 (2019).
- Tartara, L. Soliton control by a weak dispersive pulse. *J. Opt. Soc. Am. B* **32**, 395 (2015).
- Ciret, C., Leo, L., Kuyken, B., Roelkens, G. & Gorza, S.-G. Observation of an optical event horizon in a silicon-on-insulator photonic wire waveguide. *Opt. Express* **24**, 114–124 (2016).
- Herrmann, J. et al. Experimental evidence for supercontinuum generation by fission of higher-order solitons in photonic fibers. *Phys. Rev. Lett.* **88**, 173901 (2002).
- Dudley, J. M. et al. Supercontinuum generation in air-silica microstructured fibers with nanosecond and femtosecond pulse pumping. *J. Opt. Soc. Am. B* **19**, 765 (2002).
- Demircan, A. & Bandelow, U. Analysis of the interplay between soliton fission and modulation instability in supercontinuum generation. *Appl. Phys. B* **86**, 31–39 (2007).
- Husakou, A. V. & Herrmann, J. Supercontinuum generation of higher-order solitons by fission in photonic crystal fibers. *Phys. Rev. Lett.* **87**, 203901 (2001).
- Dudley, J. M. & Taylor, R. Ten years of nonlinear optics in photonic crystal fibre. *Nat. Photon.* **3**, 85–90 (2009).
- Gordon, J. P. Theory of the soliton self-frequency shift. *Opt. Lett.* **11**, 662–664 (1986).
- Mitschke, F. M. & Mollenauer, L. F. Discovery of the soliton self-frequency shift. *Opt. Lett.* **11**, 659–661 (1986).
- Amiranashvili, S. & Demircan, A. Hamiltonian structure of propagation equations for ultrashort optical pulses. *Phys. Rev. A* **82**, 013812 (2010).
- Demircan, A., Amiranashvili, S., Brée, C., Morgner, U. & Steinmeyer, G. Supercontinuum generation by multiple scatterings at a group velocity horizon. *Opt. Exp.* **22**, 3866–3879 (2014).
- Brée, C., Steinmeyer, G., Babushkin, I., Morgner, U. & Demircan, A. Controlling formation and suppression of fiber-optical rogue waves. *Opt. Lett.* **41**, 3515 (2016).
- Babushkin, I. et al. The effect of chirp on pulse compression at a group velocity horizon. *IEEE Photon. J.* **8**, 7803113 (2016).

### Acknowledgements

Deutsche Forschungsgemeinschaft (DFG) (project MO 850-19/2), Germany's Excellence Strategy within the Cluster Excellence PhoenixD (EXC 2122, Project ID 390833453). R.A. thanks Russian Science Foundation (project 19-72-00012) for the financial support. We acknowledge support by the Open Access Publication Fund of Humboldt-Universität zu Berlin. Open access funding provided by Projekt DEAL.

### Author contributions

O.M., C.B., R.A., S.W., I.B., D.S., and A.D. performed the theoretical investigations and the formal analysis. A.T. and A.P. built up the experimental setup and performed the experimental investigation. G.S. and U.M. provided resources and supervised the experimental investigation. All authors interpreted the data, discussed the results, and contributed to the final paper. A.D. conceived the idea and supervised the project throughout.

### Competing interests

The authors declare no competing interests.

### Additional information

Supplementary information is available for this paper at <https://doi.org/10.1038/s42005-020-00414-1>.

Correspondence and requests for materials should be addressed to G.S. or A.D.

Reprints and permission information is available at <http://www.nature.com/reprints>

**Publisher's note** Springer Nature remains neutral with regard to jurisdictional claims in published maps and institutional affiliations.



**Open Access** This article is licensed under a Creative Commons Attribution 4.0 International License, which permits use, sharing, adaptation, distribution and reproduction in any medium or format, as long as you give appropriate credit to the original author(s) and the source, provide a link to the Creative Commons license, and indicate if changes were made. The images or other third party material in this article are included in the article's Creative Commons license, unless indicated otherwise in a credit line to the material. If material is not included in the article's Creative Commons license and your intended use is not permitted by statutory regulation or exceeds the permitted use, you will need to obtain permission directly from the copyright holder. To view a copy of this license, visit <http://creativecommons.org/licenses/by/4.0/>.

© The Author(s) 2020